THERMOSCIENCES DIVISION
STANFORD UNIVERSITY
MECHANICAL ENGINEERING DEPARTMENT
STANFORD, CALIFORNIA
94305-3030

September 29, 1989
ref: C635

Dr. Spiro G. Lekoudis
Office of Naval Research
Mechanics Division Code 1132F
800 N. Quincy Street
Arlington, VA 22217-5000

Dear Spiro:

Enclosed please find:

1) A copy of the Annual Progress Report on our contract (N00014-88-K-0592)

2) Yearly Research Summary requested by Mike Reischman.

Please pass on to Mike item 2).

Thank you very much for your consideration. We hope to see you in November.

Best regards,
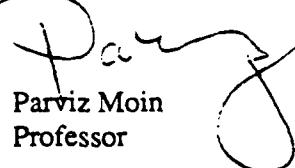
Parviz Moin
Professor

ds
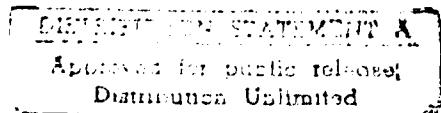
89 10 30 229

Direct Numerical Simulation of Aerodynamic Noise

First Annual Progress Report

ONR Grant N00014-88-K-0592

Principal Investigator : Parviz Moin

Sr. Research Associate : Sanjiva K. Lele

Research Assistant : Tim Colonius

September 28, 1989

Department of Mechanical Engineering

Stanford University

Stanford, CA 94305

Direct Numerical Simulation of Aerodynamic Noise
ONR Grant N00014-88-K-0592

Principal Investigator : Parviz Moin

Sr. Research Associate : Sanjiva K. Lele

Research Assistant : Tim Colonius

OBJECTIVES

Direct Numerical Simulation of Aerodynamic Noise is a part of an overall research program in compressible turbulence being conducted at the Center for Turbulence Research. The program includes study of the physics of compressible turbulence, shock-turbulence interactions, reacting flows with heat release, and aerodynamic sound generation in shear flows.

The objective of the work in aerodynamic sound generation is to use direct numerical simulations as a tool to study the noise generation processes directly. Specifically, we wish to answer the following questions:

1. Can one relate particular flow regions and events to the far-field noise ?

2. What regions are the dominant contributors to the far-field noise?

3. What is the role played by pairing process in noise generation?

4. How important are the small scales to the noise generation?

5. What processes control the far-field directivity pattern?

In order to answer these questions in shear flows, we are first studying the acoustics of simple "building-block" flows. The discussion below presents recent results obtained for one of the "building-block" flows, the scattering of sound by a vortex. A short discussion of numerical accuracy is also given. Finally, results are presented for aerodynamic sound generation from a 2-d temporal mixing-layer.

DISCUSSION

1. Scattering of Sound by a Vortex.

A 2-d compressible vortex is irradiated with small amplitude $(10^{-5}$ relative to the maximum vortex velocity) plane sound waves. The scattered sound waves are directly measured and analyzed. The flow is of interest as a model of scattering of sound by vortices in shear flows, and is also of technical interest in detection of trailing vortices from aircraft or other moving objects.

The vortex is nearly inviscid with a Reynolds number based on circulation and kinematic viscosity of 10^5, and we restrict our attention to cases where the ratio of the wavelength of the incident sound is comparable with the size of the vortex (The results reported have a ratio of 4). Intensity and phase of the scattered wave field and their dependence on Mach Number have been computed. Figure 1 shows a typical result (M = .125) of the root mean square pressure level of the scattered wave. There is preferred scattering in the forward direction, and the maximum scattering occurs at an angle of about -30 degrees from the direction of incident propagation. Scattering in the backward direction is at least an order of magnitude smaller than in the forward direction.

The scattered amplitude integrated over all angles multiplied by the radius raised to the .5 power is plotted as a function of radius for 4 different Mach Numbers in Figure 2. The pressure amplitude should scale with $r^{-.5}$ in the far field (Monopole radiation in two dimensions decays like $r^{-.5}$) and therefore the curves asymptote to a constant value in the far field. The approach to far- field behavior appears to occur on a length scale which scales with the wavelength of the incident sound waves. This adjustment length is only very weakly dependant on Mach Number. Moreover, it is found that as the Mach Number approaches zero, the far-field intensity scales with the intensity of the incident waves as predicted by aero- acoustic theory. When un-normalized, the data obeys a Mach Number squared power law, as is seen in Figure 3. In Figure 4, the abscissa has been divided by the Mach Number squared to show the deviation from the incompressible aero-acoustic limit. The deviations at M = .25 and M = .5 are 3% and 25% respectively.

The scattering from the compressible vortex has contributions from two main sources: interactions of the incident wave with the velocity field, and interactions of the incident wave with the density gradient. To separate the effects, scattering of plane waves by a density inhomogeneity alone were computed. The scattering amplitude is found to be an order of magnitude less than that from the vortex, suggesting that the density inhomogeneity is not an important scattering mechanism in the vortex.

2. Numerical Accuracy

Another objective of the reported studies was validation of the numerical method used to compute the flows. Sound fluctuations are very small compared to the flow fields, and extreme care must be taken to insure that numerical errors are kept several orders of magnitude smaller than sound fluctuations.

In resolving the sound waves, two types of numerical errors are important–phase and amplitude error resulting from the time-marching scheme, and spurious reflection of waves at the artificial numerical boundaries. Simulation of the scattering from a vortex presents a difficult test case. Since the vortex velocity decays like $1/r$, the vortex has infinite energy, and numerical boundaries must account for inflow and outflow of mass, momentum and energy. The boundary must also be capable of exciting an incoming sound wave, and still remain non-reflecting to out-going sound waves.

As a test, the vortex was removed from the domain, and left and right-going sound waves were generated at the boundaries. For small amplitude waves the exact solution is well known, viz

$$u = f(x - ct) + g(x + ct).$$

This exact solution is subtracted from simulation results, quantifying phase and amplitude error, and spurious reflection error. A time history of the error is shown in Figure 5. For the same spatial and temporal resolution as used in simulating the vortex scattering, the error was about one thousandth of the scattered wave amplitude, which is sufficiently small.

3

3. Temporally Evolving Mixing Layer

Mixing layer flows are known to possess organized vortices (ref. 1). The formation of vortices and their subsequent merger into larger vortices causes the layer to grow (refs. 1-3). It is common to introduce an idealization of the mixing layer flow (in a frame of reference moving with the vortices) where periodic boundary conditions are posed in the flow direction. The temporally evolving mixing layer flow contains many aspects of the spatially evolving mixing layers. The acoustic radiation from temporally evolving mixing layers is studied here. The simulations use periodic boundary conditions in the flow direction (x) and non-reflecting boundary conditions (ref. 4) in the shearing direction (y) at a large distance from the shear layer. Following the experiments of Papamoschou and Roshko (ref. 5), previous numerical investigations (refs. 6-7) and results of linear stability calculations (refs. 7-9) the effects of compressibility are characterized by a convective Mach number, M_c, viz. the Mach number defined in a frame of reference moving with the dominant eddies of the flow.

Instability in the hyperbolic tangent mean velocity profile is initiated by a means of small (1% peak amplitude) incompressible disturbance confined within the shear layer. In the numerical experiments described here the initial v disturbance has the form

$$v(x,y) = f(y)(a_1 cos(\frac{2\pi x}{\lambda_x}) + a_2 cos(\frac{\pi x}{\lambda_x} + \phi)),$$

where $f(y)$ is a Gaussian profile confined to the shear layer, ϕ is the phase difference between the fundamental and the sub- harmonic disturbances. The wavelength of the fundamental disturbance scaled with the initial vorticity thickness, λ_x, is typically chosen to be 12. Simulations were also conducted where the domain size was chosen to match the most unstable wavelength. All results presented here (with fixed domain size) were also found to hold in these latter simulations. In the simulations discussed here the two streams forming the mixing layer were taken to have the same static temperature.

For the results discussed here the thickness is normalized by the initial vorticity thickness δ_{ω_0}, distances are normalized by 10 δ_{ω_0} and time is normalized by $\frac{10\delta_{\omega_0}}{U_1 - U_c}$. The simulations are conducted in a frame of reference moving with $U_c = \frac{a_1 U_2 + a_2 U_1}{a_1 + a_2}$ where a_1 and a_2 are the sound speeds in the two streams.

4

It is also convenient to further rescale the variables characterizing the far-field noise. This rescaling is based upon the expected Mach number dependence at low Mach numbers (ref. 10). The pressure is normalized as $\frac{p/p_\infty - 1}{M_c^3}$, velocity associated with outgoing sound waves as $\frac{v/a_1}{M_c^3}$, and acoustic flux in terms of these normalized values.

Acoustic Radiation

In the temporally evolving mixing layer the radiated acoustic power is a function of the evolution time. In the following time histories of the hydrodynamic variables as well as the acoustic variables (at a shifted time to account for the travel time for the acoustic signal) are presented. By this process the relation between the radiated sound and the hydrodynamic evolution of the flow may be inferred. The hydrodynamic variables are normalized with the velocity difference and the convective time scale.

In figure-6 the time histories of the momentum thickness, Reynolds stress at the centerline and integrated energy in the v fluctuations are shown. Three cases are plotted on this figure, viz. $M_c = 0.05$ (solid), 0.1 (dashed) and 0.2 (chain). The initial disturbance in the three cases were identical and excited the layer to roll up. It is evident from this figure that the compressibility effect inherent in M_c disappears as $M_c \to 0$. The growth rate of the mixing layer, the Reynolds stresses generated by the roll up and the disturbance energy level become independent of M_c, showing a clear approach to an incompressible hydrodynamic evolution. In figure-7 the time histories of the rescaled acoustical quantities are shown. The quantities displayed include the scaled pressure and velocity signal in the far- field and the calculated acoustic flux radiated from the layer. Also shown is the time history of the rate of work done by the mean flow (integrated over the domain). It may be seen that as the layer roll up to form vortices and its thickness increases a compression wave is generated. This compression wave is followed by a weak expansion wave during the time the flow relaxes. The time history of the hydrodynamic work is very much like the far-field signal, showing a good correlation between generation of fluctuation energy and the acoustic radiation. By using aero-acoustic theory (ref. 10) the far-field noise can be calculated from the hydrodynamic evolution of the flow. These may be compared to the direct 'measurement' of the far-field noise. These comparisons

will be presented later. It may be noted that the scaled acoustic variables (in fig. 7) also become independent of M_c as $M_c \to 0$, as expected from the aero-acoustic theory. In figure-8 and 9 time histories similar to figure-6 and 7 are shown for roll up at higher M_c. The three cases plotted have $M_c = 0.2$ (solid), 0.38 (dashed) and 0.6 (chain). It may be noted that as M_c is increased the roll up process becomes progressively slower, generating weaker fluctuations and extracting less energy from the mean flow. It may also be noted that at late times the hydrodynamic variables develop oscillations which damp slowly. The scaled acoustic variables in figure-9 show that the far-field radiation departs significantly from the $M_c \to 0$ scaling at $M_c = 0.38$ (the scaling over predicts the radiated flux by as much as 100%). The expansion wave is almost equal to the compression wave and this cycle is repeated in time. In this cyclic process the Reynolds stress oscillates around zero thus the work done by the mean flow changes sign with time. This oscillatory behavior is associated with the shape oscillations of the elliptical vortices in the mixing layer.

Results obtained from the simulations that include the sub-harmonic disturbance are shown in figure-10 and 11. In these figures three cases all with $M_c = 0.4$ are shown. The cases correspond to forcing the layer with a) fundamental alone (solid line), b) sub-harmonic alone (dashed line) and c) fundamental and sub-harmonic together (chained line). It may be seen that the initial development of the flow in case (c) is much like case (a). This corresponds to the roll up stage. There is good correspondence in the radiated sound also. Further in time, case (c) shows vortex pairing. This process generates large acoustic radiation (about 8-9 times that due to fundamental roll up). The time characteristics of the acoustic signal are also quite different. The compression wave generated by the pairing event is almost equal in magnitude to the expansion wave generated by the relaxation subsequent to the pairing. In figure-11 the far-field acoustic pressure calculated from a (modified) aero-acoustic theory is also shown for the three cases. This may be compared to the far-field pressure 'measured' in the computations. The agreement between the two is excellent (the maximum difference is about 1-2 %).

Finally, an example of roll up and pairing at $M_c = 0.6$ is presented in figure-12. The roll up, pairing and nutation processes can be identified in the time histories. The roll up and pairing cause the layer thickness to increase and generate a compression wave.

6

Subsequent to pairing, the nutation of the vortices causes a periodic energy exchange between the vortices and the mean flow. This process generates a series of compression and expansion waves which carry acoustic energy away from the layer. The numerical simulations show that the nutation frequency is close to $\frac{\omega}{2}$, where ω is the peak vorticity. The primary effect damping the nutations appears to be viscous dissipation.

Mach Number scaling for the Far-Field

Lighthill (ref. 11) in his pioneering work on aerodynamic noise showed that acoustic power emitted by a jet (into 3-d space) is proportional to the jet speed to the eighth power (for subsonic jets). He also showed that the experimental measurements were consistent with this M^8 dependence of the acoustic flux. For supersonic jets the power emitted rises more gradually with the Mach number and a power law exponent of 3 seems to fit the data. Later it was shown by Muller and Obermeier (ref. 12) that for compact sources in two dimensions the power emitted is proportional to M^7. Ffowcs Williams (ref. 10) showed that for a mth order pole (with $m = 0, 1, 2$ for monopole, dipole and quadrupole in n space dimensions the power emitted is proportional to M^{2m+n+1} for low Mach number. Thus the quadrupole radiation ($m = 2$) from temporally evolving shear layers ($n = 1$ due to spatial periodicity) is expected to have a M^6 dependence. Such a power law has also been proposed for the low frequency emission from localized sources of turbulence (turbulent spots, slugs and bursts) in pipes and ducts (ref. 13).

While the aero-acoustic theory has lead to useful scaling relations it is, generally, unable to provide the value of the coefficient in the power laws. This is because of the nonlinear character of the hydrodynamic flow which generates the noise field. Only for highly idealized flows it becomes possible to calculated the noise field from this asymptotic theory. Another limitation of the aero-acoustic theory is that it is unable to provide a self-consistent derivation of its range of validity. Thus without experimental data on the measured noise field, the theory is not capable of providing an estimate of uncertainty. The present simulations overcome both of these difficulties for the flows that have been simulated. From the 'measured' far-field noise in the simulations it is possible to assess

both the coefficient in the power law as well as error estimates on its range of validity. These results are briefly presented here.

In figure-13 the peak level of the far-field acoustic flux (in time) is plotted against the Mach number M_c on a log-log plot. Data is included from four different cases. 1) fundamental roll-up (circles), 2) sub-harmonic roll-up (triangles), 3) vortex pairing (i.e. fundamental and sub-harmonic in phase) (pluses) and 4) vortex shredding (fundamental and sub-harmonic with a phase difference of $\frac{\pi}{2}$ (cross). It may be seen that in all cases the power emitted rises rapidly as the Mach number M_c is increased. This increase in the radiated power is proportional to M_c^6. It appears that this power law (expected from the aero-acoustic theory) may be adequate up to M_c of 0.6. In figure-14 the same data is re-plotted with the acoustic flux normalized by M_c^6. This way it is clearly established that the emitted power does indeed asymptote to M_c^6 power law. The constant factor involved in the power law is estimated to be 0.014, 0.046 and 0.101 for the three cases. It may be further seen that even at M_c of 0.2 there is a 25% departure from the power law. At M_c of 0.5 this departure is larger than 100%. These departures are difficult to assess from figure-13 since a factor of two change in the Mach number produces a 36 fold change in the acoustic power. It may be noted from these low Mach number asymptotes that vortex pairing radiated about 8-9 times the power radiated from the fundamental roll up.

As M_c increases the acoustic power radiated increases less rapidly. This is due to the stabilizing effect of compressibility on the vortex roll up and pairing. This stabilizing effect is missed out in the conventional aero-acoustic theory. It is ,however, possible to modify the aero-acoustic theory by using the quadrupole sound sources from the simulations. As documented elsewhere (see ref. 6 for details) the hydrodynamic evolution of the flow is progressively slower for M_c larger than 0.4 thus progressively weaker sound sources are anticipated to emerge. When the far field sound is computed from this modified aero-acoustics, once again a rather good agreement between the 'measurements' and the theory is obtained (as documented in figure-11). For example at $M_c = 0.6$ the (incompressible) aero-acoustic theory would be in error by more than 100% while using the numerical aero-acoustics the discrepancy is reduced to 2-3%.

8

Acoustic efficiency

It is possible to calculate the acoustic efficiency of the aerodynamic noise sources. For the purposes of defining the acoustic efficiency we have chosen to normalize the acoustic power emitted to the far-field by the rate of extraction of energy from the mean flow. As discussed earlier at low M_c the hydrodynamic evolution of the flow becomes independent of the Mach number, while the acoustic power emitted is proportional to M_c^6. These imply that the acoustic efficiency decreases as M_c^3 for low Mach number. The coefficient in this power law dependence has been evaluated to be 0.11 and 0.36 for the fundamental roll up and pairing cases. It is seen that at M_c of 0.2 only 0.08% (roll up), 0.3% (pairing) of the energy extracted is converted to noise. This fraction steadily increases with Mach number, but even at M_c of 0.6 only 0.4% (roll up), 1.7% (pairing) of the energy extracted is converted to sound. Based on these estimates it is suggested that in the transitional range of M_c where the compressibility effect slow down the growth of the layer, this effect arises primarily from the direct compressibility effect on the eddies and not from eddies losing their energy to the sound field as proposed by some investigators.

CONCLUSIONS

Acoustic Radiation from Temporal Mixing Layers

1. Verification that hydrodynamic evolution approaches the incompressible limit as $M_c \rightarrow 0$, where M_c is the convective Mach number.

2. For low M_c the measured far-field radiation arising from vortex roll up and pairing behaves like M_c^6 as expected from aero-acoustic theory.

3. Deviations from the incompressible aero-acoustic limit are obtained as a function of M_c. At M_c of 0.2 and 0.5 these deviations are 25% and 100%, respectively. The deviations are reduced to 1-2% when the 'exact' source field is used from the simulations.

4. Peak noise generated by vortex pairing is about 8-9 times the peak noise generated by vortex roll up.

5. Acoustic efficiency is quantified by the simulations. It scales with M_c^3 for low M_c. Even at M_c of 0.6 less than 2% of the energy extracted from the mean flow is radiated.

6. The slower growth of the compressible mixing layer is not due to the increased acoustic radiation.

Acoustic Scattering from a Vortex

1. Intensity and phase of the scattered field and their dependence on vortex Mach number M_v and $\frac{\lambda_i}{R_v}$ is obtained.

2. At low M_v far-field intensity scales with the intensity of the incident waves (as predicted by aero- acoustic theory).

3. Deviations from the aero-acoustic limit are quantified. At M_v of 0.25 and 0.5 the deviations are 3% and 25%.

4. Scattering arising from the density inhomogeneity in the vortex is an order of magnitude smaller than the overall scattering.

FUTURE WORK

Our future plans are:

1. Continue studying the dynamics and acoustics of "simple" vortex flows to develop a better understanding of complex flows.

2. Computation of 3-d spatially evolving flows, in particular the near field of a circular jet and a mixing layer.

3. Computation and understanding of the far-field noise characteristics of these flows.

LIST OF FIGURES

Figure 10 Time history of hydrodynamic variables at $M_c = 0.4$; a) Momentum thickness, b) Centerline Reynolds stress, c) Integrated energy in v on linear and log scale. Solid line (fundamental alone), Dashed line (sub-harmonic alone) and chained line (fundamental and sub-harmonic together)

Figure 11 Time history of acoustic variables at $M_c = 0.4$; a) Scaled pressure, b) Calculated acoustic pressure c) Scaled v velocity, d) Reynolds stress work, e) Scaled acoustic flux Solid line (fundamental alone), Dashed line (sub-harmonic alone) and chained line (fundamental and sub-harmonic together)

Figure 12 Acoustic radiation from vortex pairing and nutation at $M_c = 0.6$; Time history of a) normalized pressure, b) normalized v velocity, c) Reynolds stress work and d) normalized acoustic flux are shown. Solid line (fundamental alone), Dashed line (fundamental and sub-harmonic together).

Figure 13 Peak acoustic flux as a function of Mach number M_c; a) fundamental roll up (circles), b) sub-harmonic roll up (triangles) c) vortex pairing (pluses) and d) vortex shredding (tearing) (cross).

Figure 14 Normalized peak acoustic flux as a function of Mach number M_c; a) fundamental roll up (circles), b) sub-harmonic roll up (triangles) c) vortex pairing (pluses) and d) vortex shredding (tearing) (cross).

REFERENCES

1 Brown, G. L. and Roshko, A. (1974) J. Fluid Mech., v. 64, p775-816.

2 Winant, C. D. and Browand, F. K. (1974) J. Fluid Mech., v. 63, p237,255.

3 Ho, C. M. and Huerre, P. (1984) Ann. Rev. Fluid Mech., v. 16, p365-424.

4 Thompson, K. W. (1987) J. Comput. Phys., v. 68, p1- 24.

5 Papamoschou, D. and Roshko, A. (1986) AIAA paper, AIAA-86-0162.

6 Lele, S. K. (1989) AIAA paper, AIAA-89-0374.

7 Sandham, N. D. and Reynolds, W. C. (1989) AIAA paper, AIAA-89-0371.

8 Ragab, S. A. and Wu, J. L. (1988) AIAA paper, AIAA- 88-0038.

9 Zhuang, M., Kubota, T. and Dimotakis, P. (1988) in Proceedings of the 1st National Fluid Dynamics Conference, Cincinnati, 88-3583-CP.

10 Ffowcs Williams, J. E. (1969) Ann. Rev. Fluid Mech., v. 1, p197-222.

11 Lighthill, M. J. (1955) Proc. R. Soc. Lond. A, v. 211, p564-587.

12 Muller, E. A. and Obermeier, F. in Proceedings of 'Fluid dynamics of rotor and fan supported aircraft at subsonic speeds, Sept. 1967 (AGARD).

13 Davies, H. G. and Ffowcs Williams, J. E. (1968) J. Fluid Mech., v. 32, p765-778.
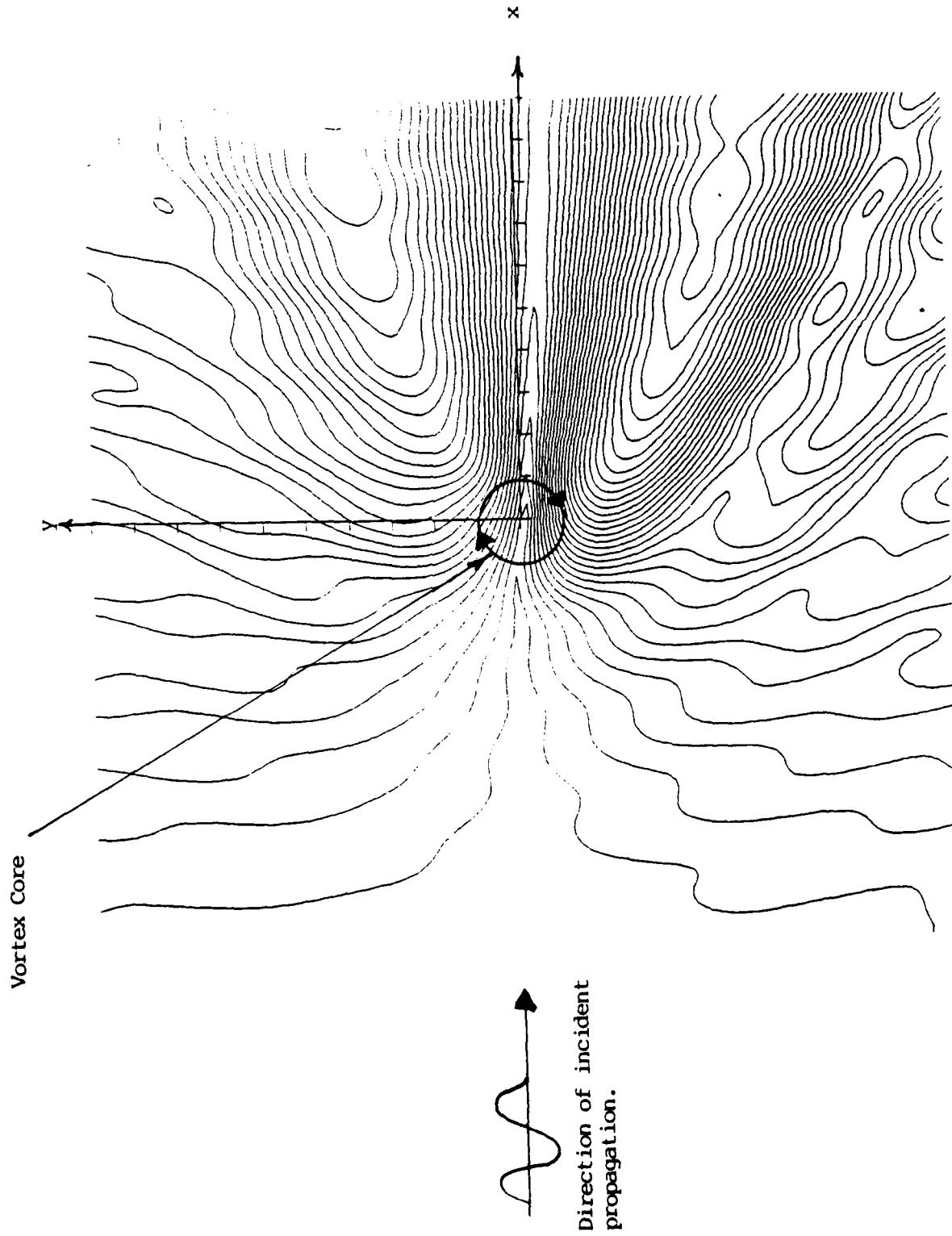
Figure 1. Iso-contours of the root mean square pressure level of the scattered wave. Contour levels: Min.=.01 Max.=.59, Increment=.02. M = .125.

Vortex Core

Direction of incident propagation.

Scattering Amplitude scaled with Amplitude of Incoming Wave

LEGEND
□ M = .0625
○ M = .125
△ M = .25
+ M = .5

Total Scattering Amplitude

Radius

Figure 2.

Mach Number Scaling

Total Far-Field Scattered Wave Amplitude

Mach Number

Figure 3.

Mach Number Scaling

Total Far-Field Scattered Wave Amplitude/Mach Number**2
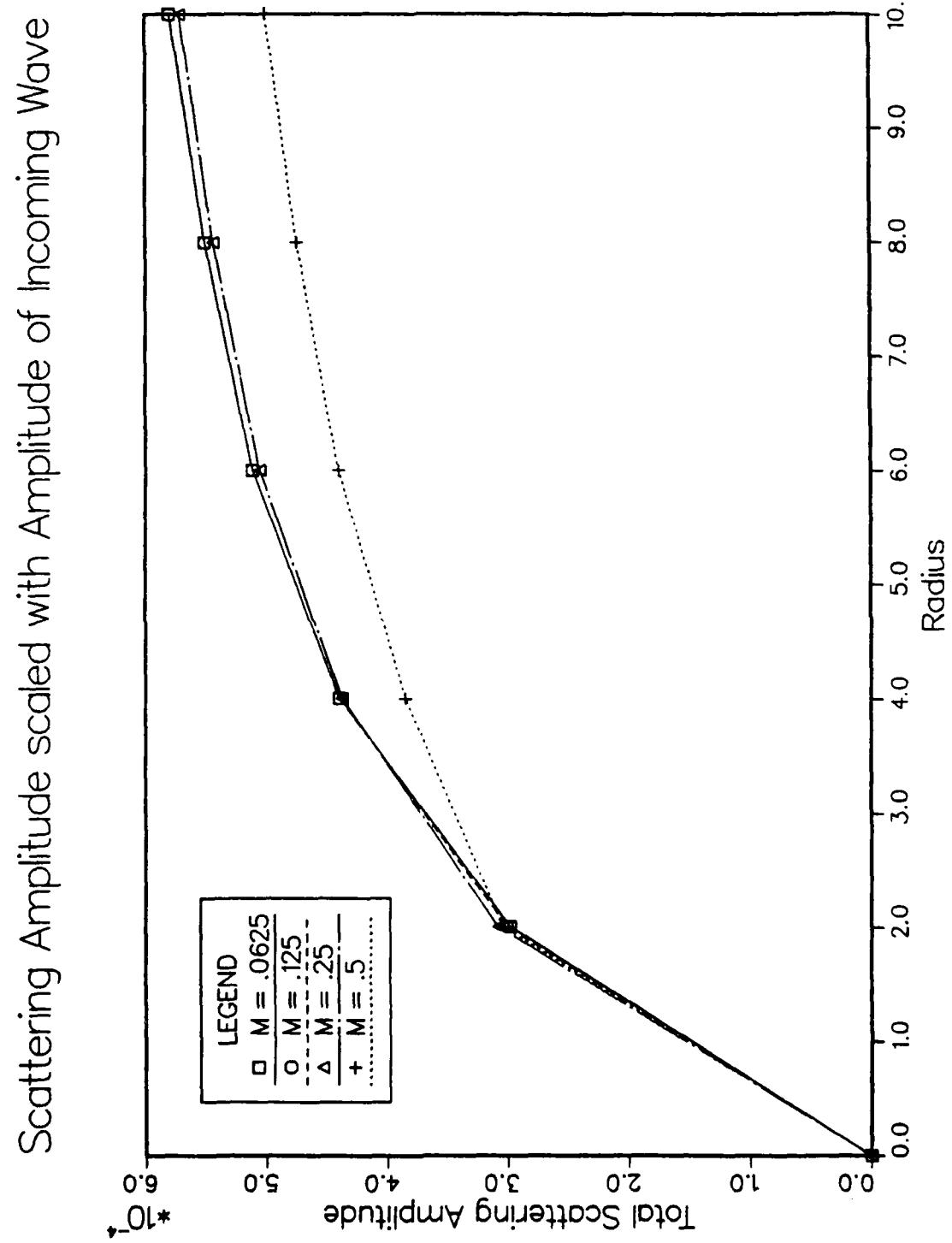
Mach Number
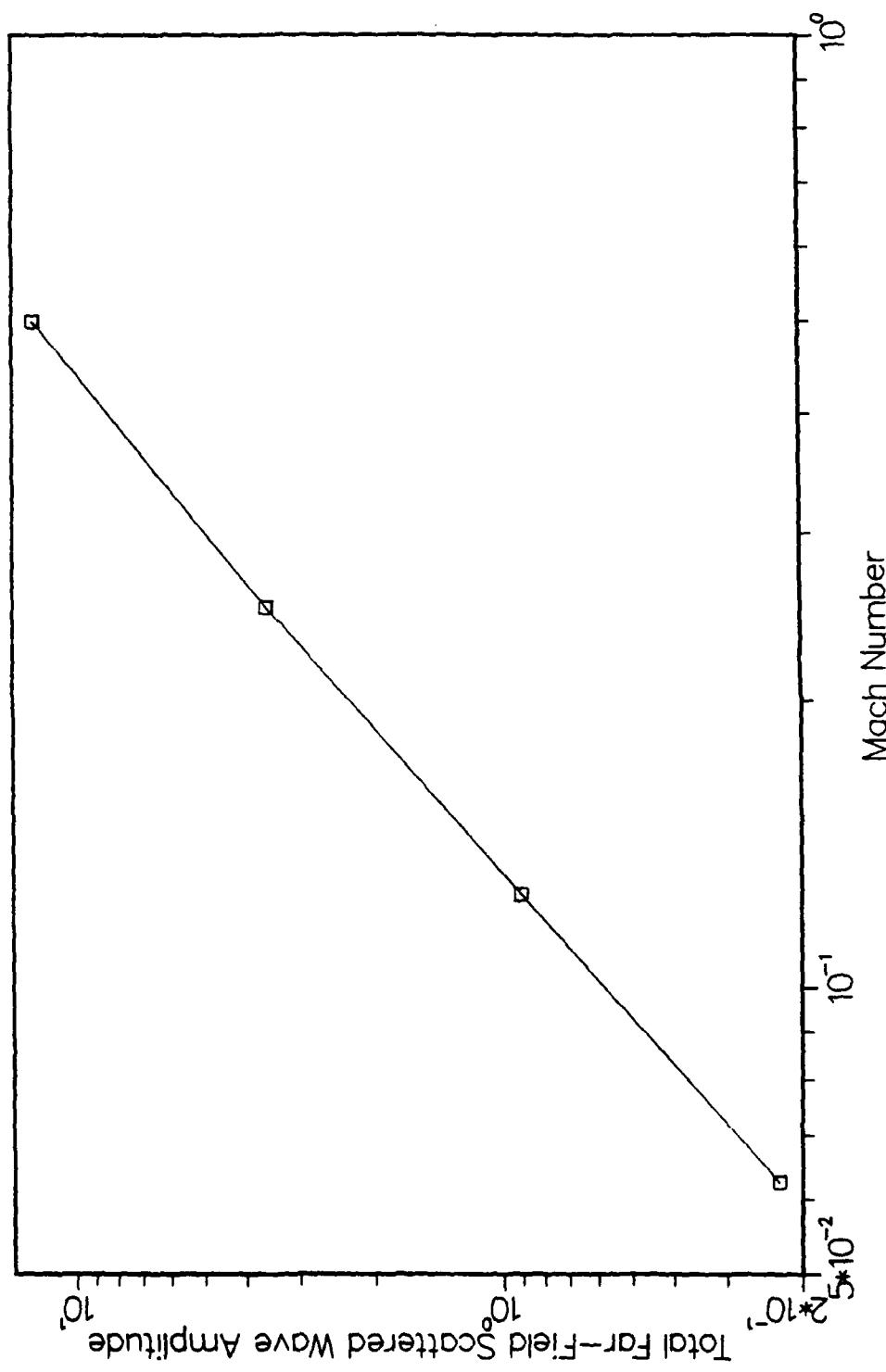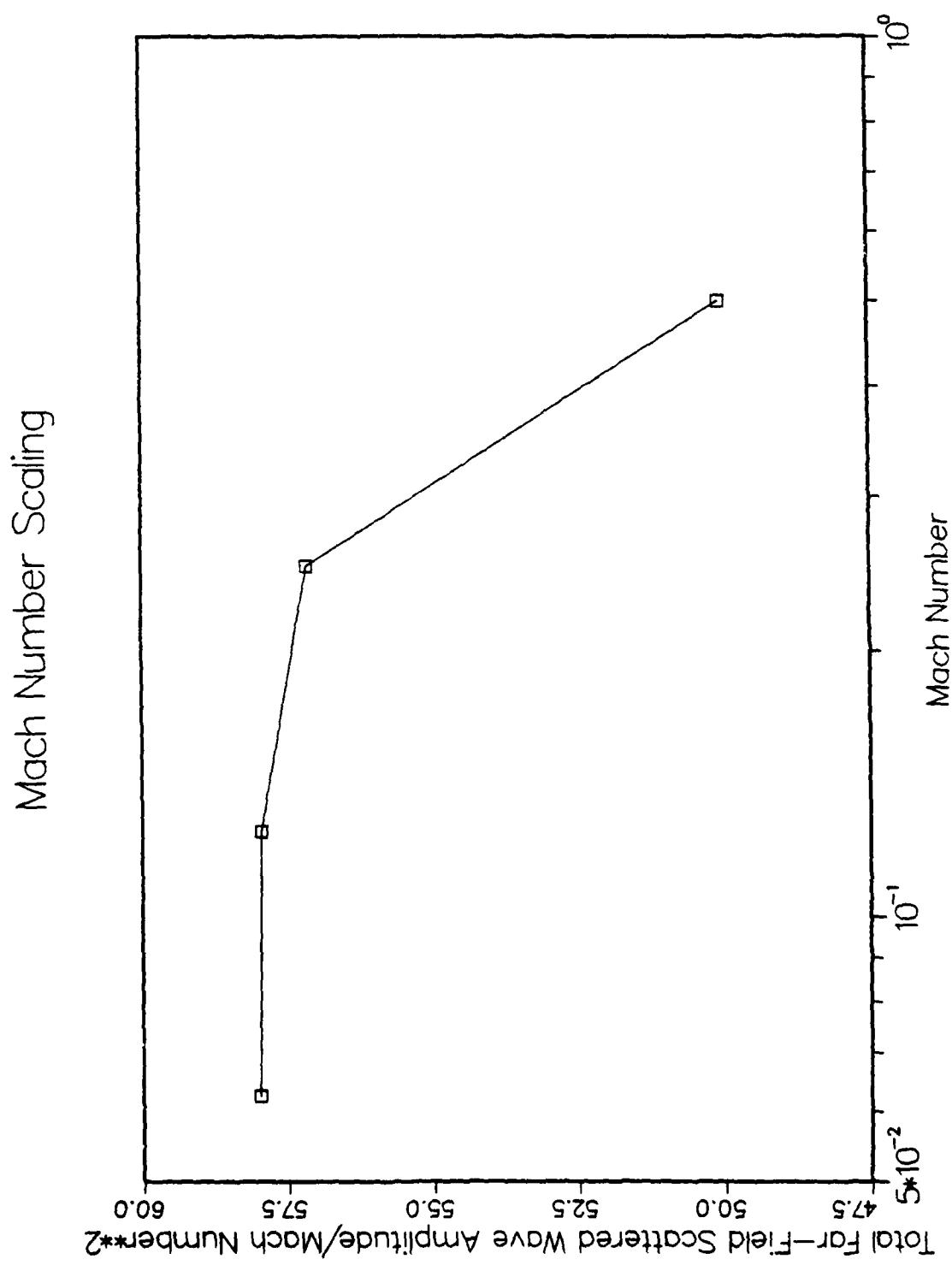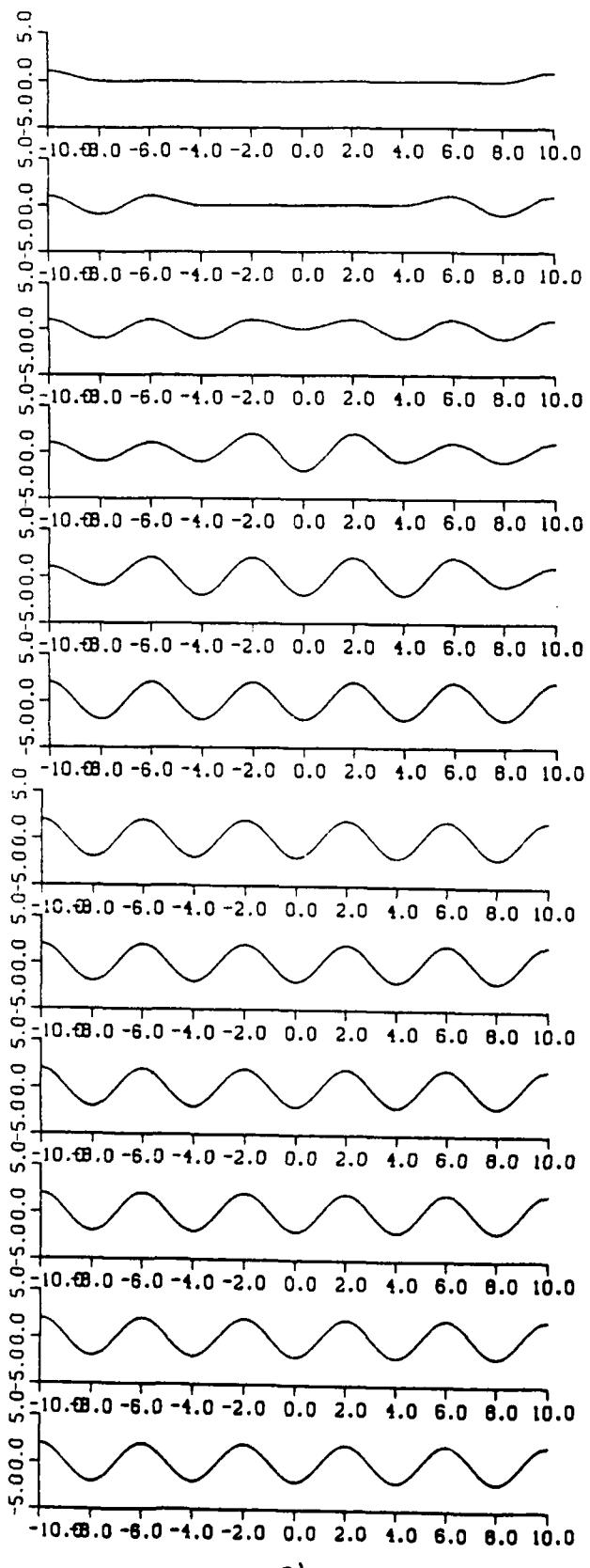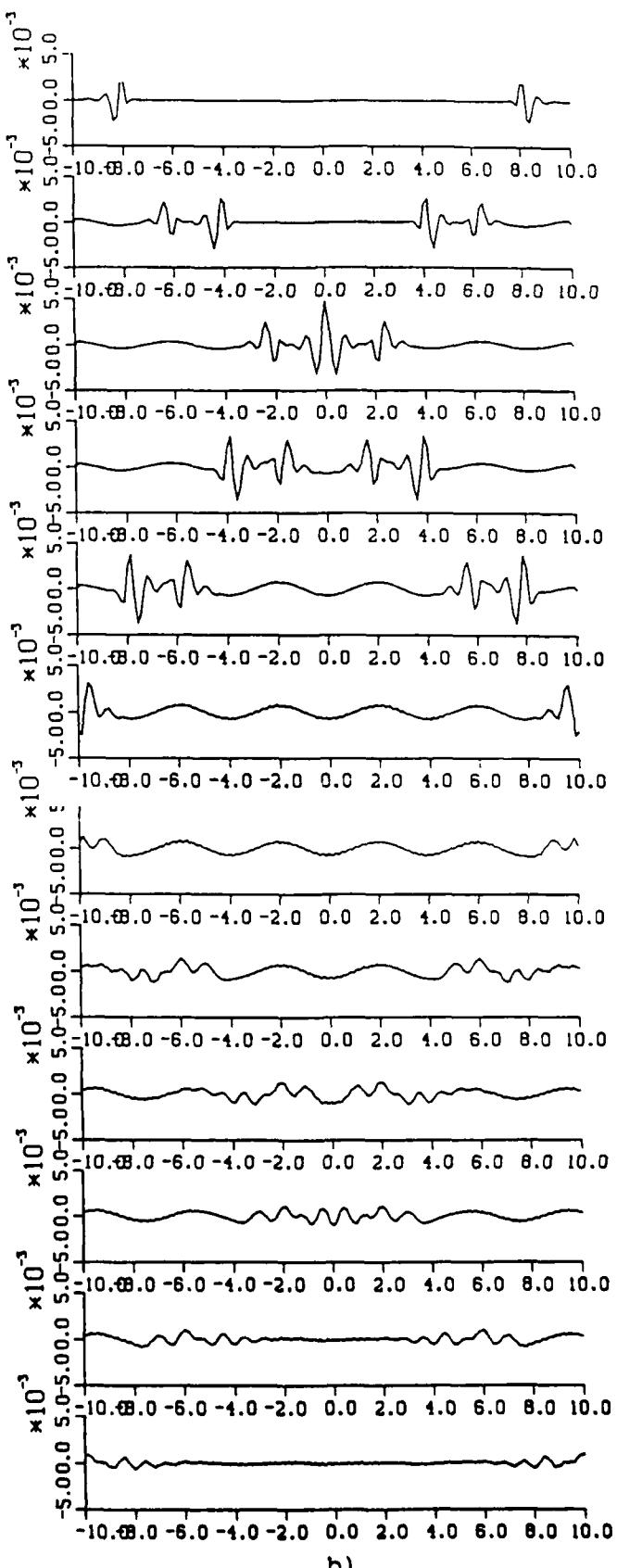
Figure 4.

a)   b)

Figure 5.   (Continued on next page.)
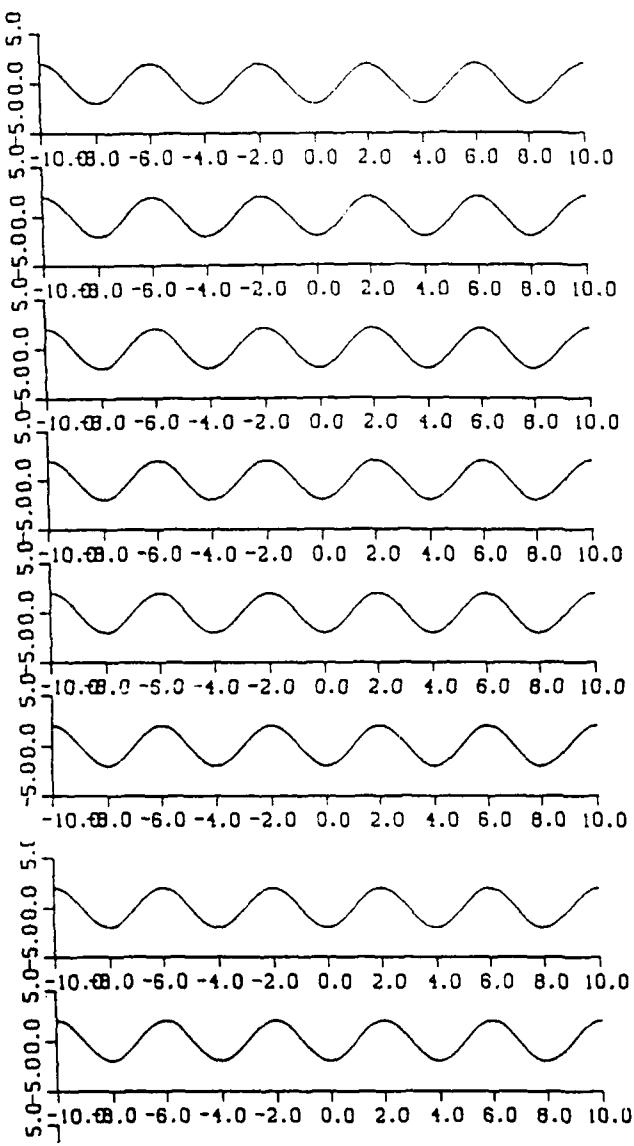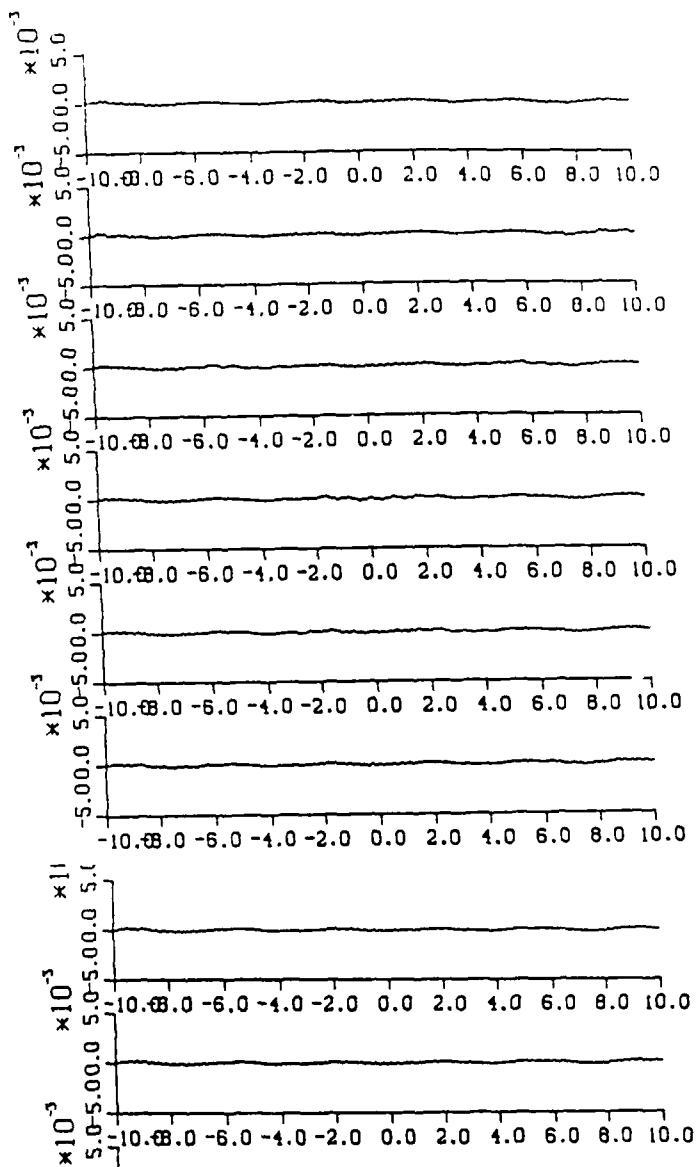
a)   b)

Figure 5. (Cont'd.) Time history of a) Numerical solution for
left and right going one-dimensional waves. and b) Error in
same numerical solution. (Numerical solution minus exact sol-
ution. Both a) and b) scaled with amplitude of wave.
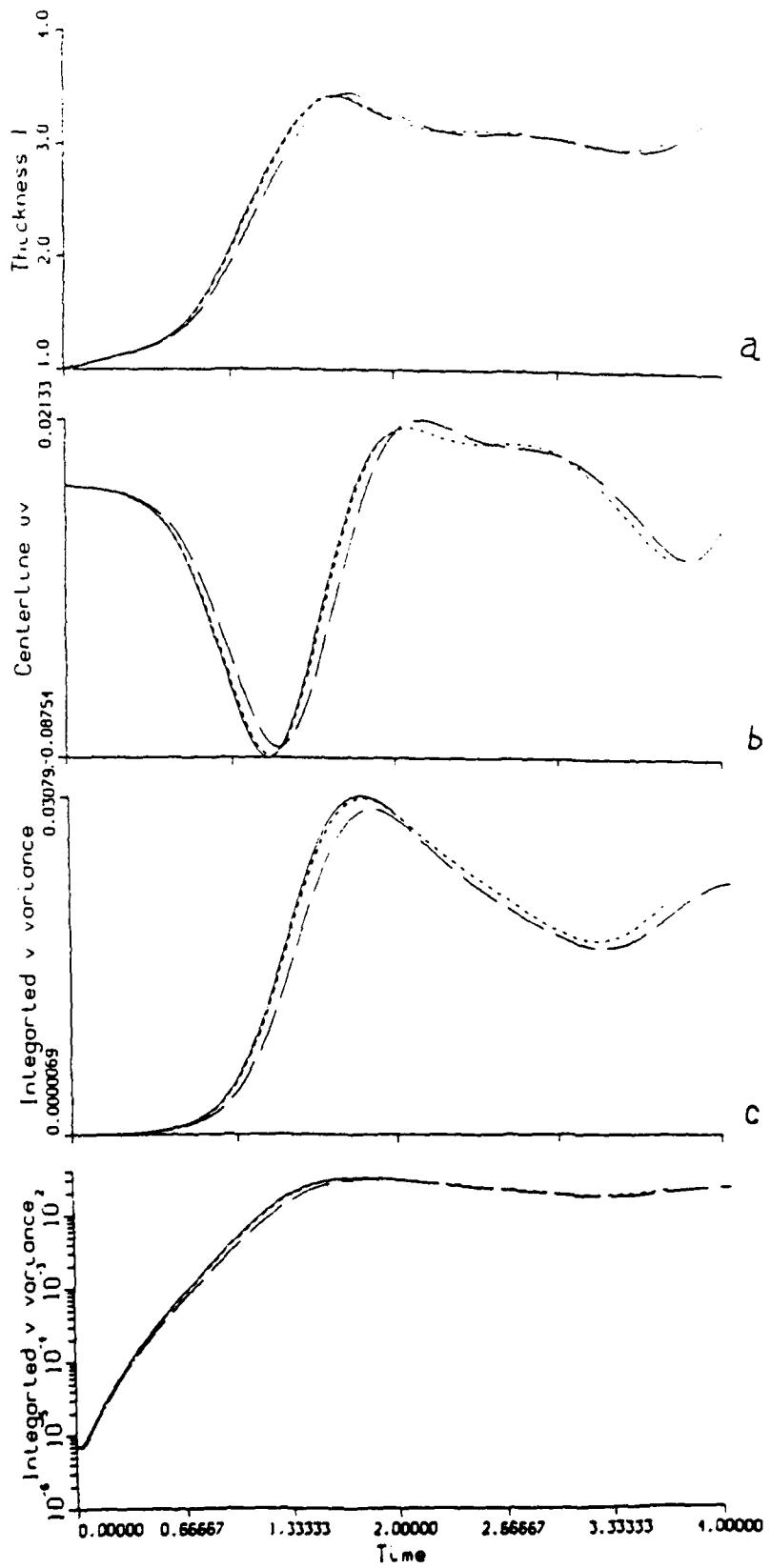
Figure 6 Time history of hydrodynamic variables for vortex roll up; a) Momentum thickne
Centerline Reynolds stress, c) Integrated energy in v on linear and log scale. Soli
($M_c = 0.05$). Dashed line ($M_c = 0.1$) and chained line ($M_c = 0.2$)
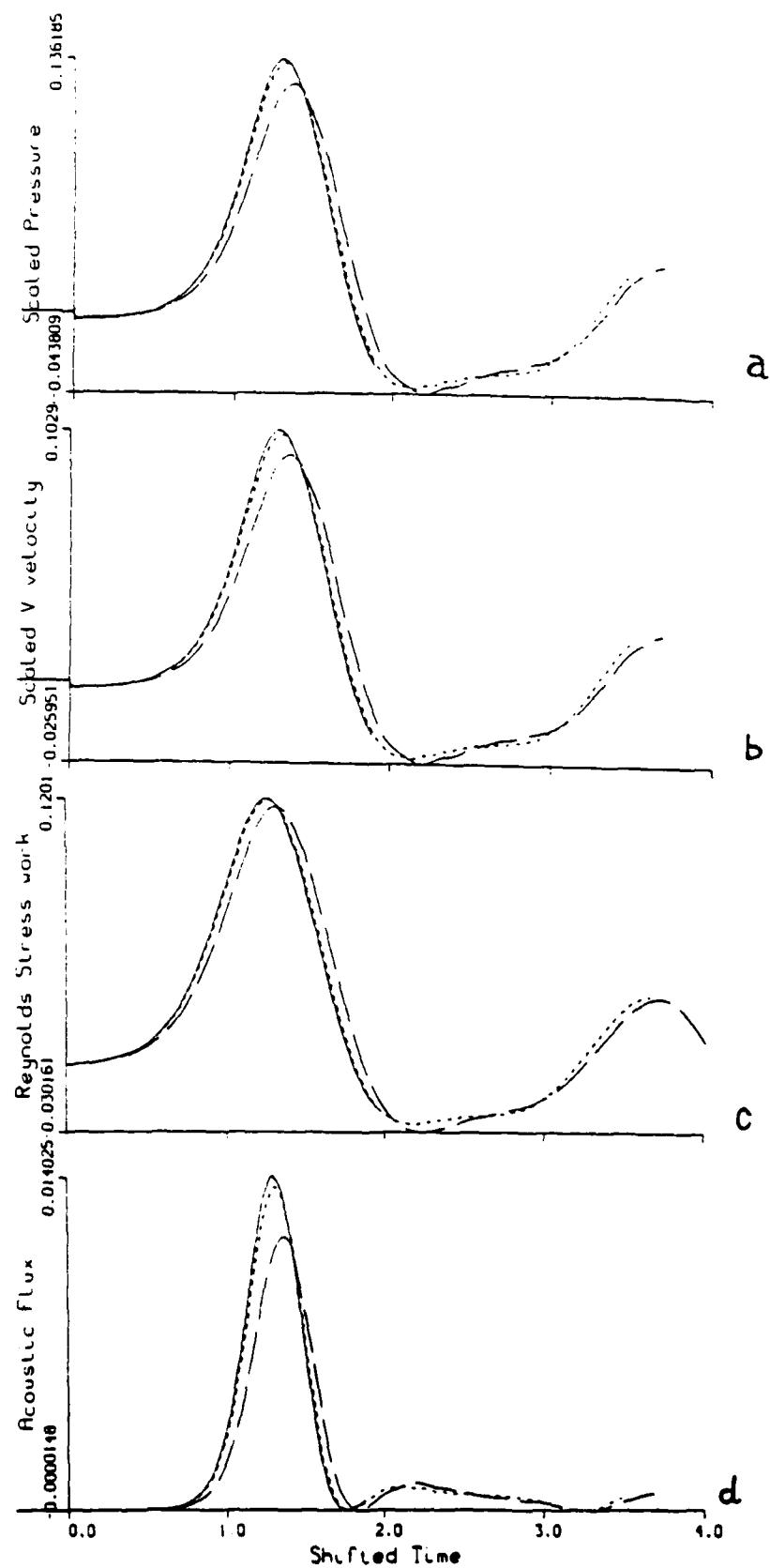
Figure 7 Time history of acoustic variables for vortex roll up; a) Scaled pressure, b) Scaled v v c) Reynolds stress work, d) Scaled acoustic flux Solid line ($M_c = 0.05$), Dashed line 0.1) and chained line ($M_c = 0.2$)
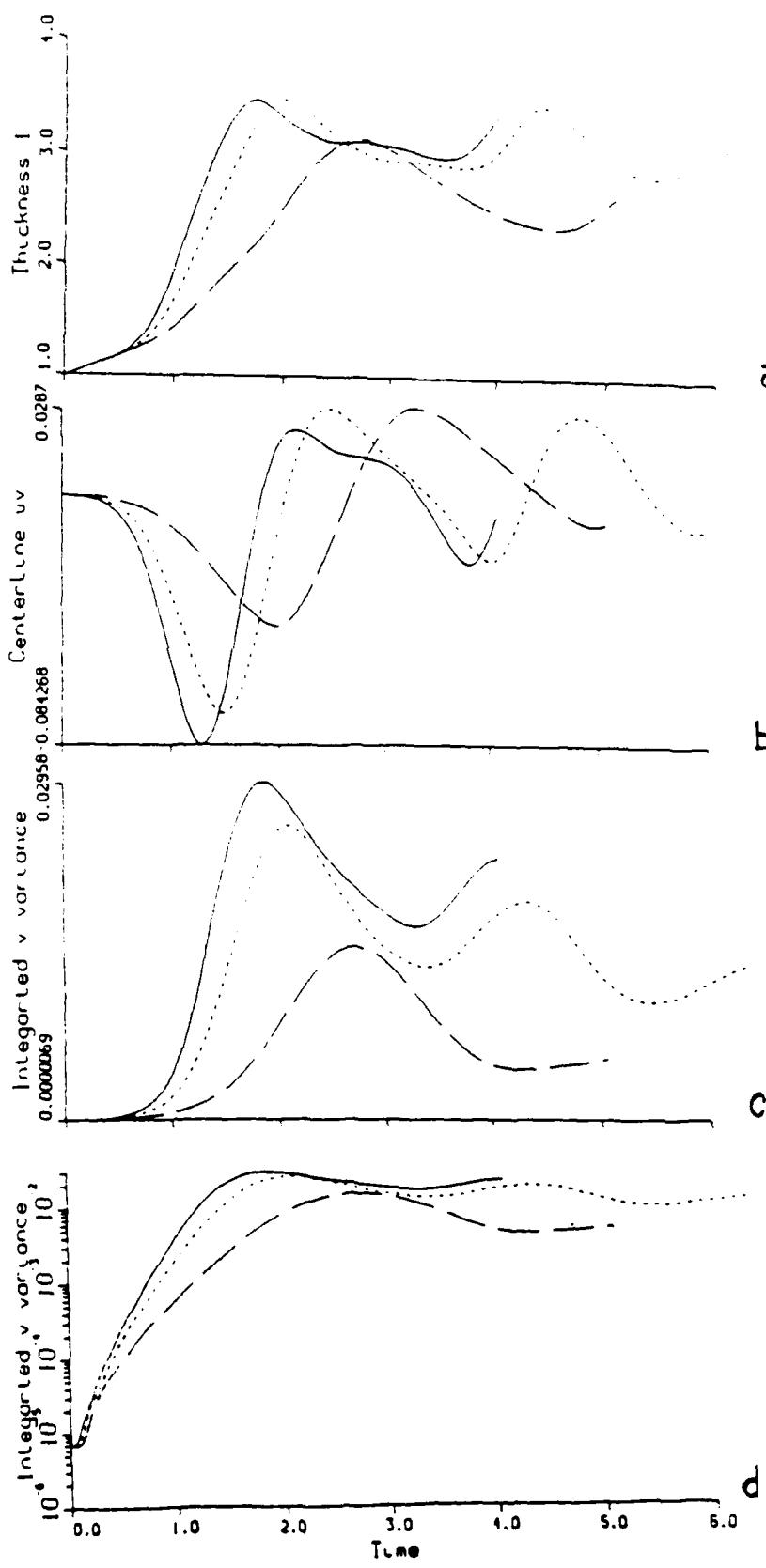
Figure 8 Time history of hydrodynamic variables for vortex roll up; a) Momentum thickn
Centerline Reynolds stress, c) Integrated energy in v on linear and log scale. Sol
($M_c = 0.2$), Dashed line ($M_c = 0.38$) and chained line ($M_c = 0.6$)
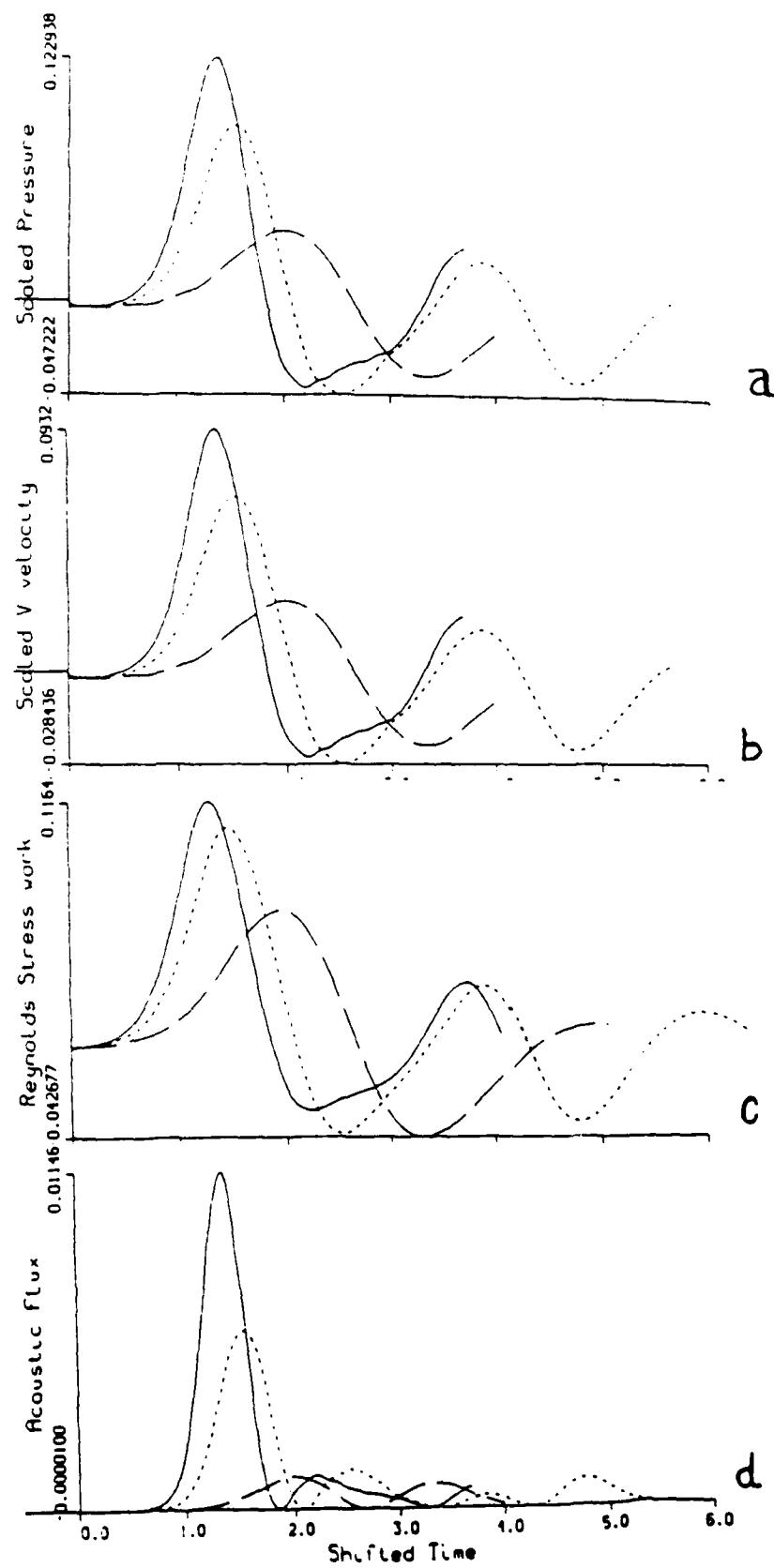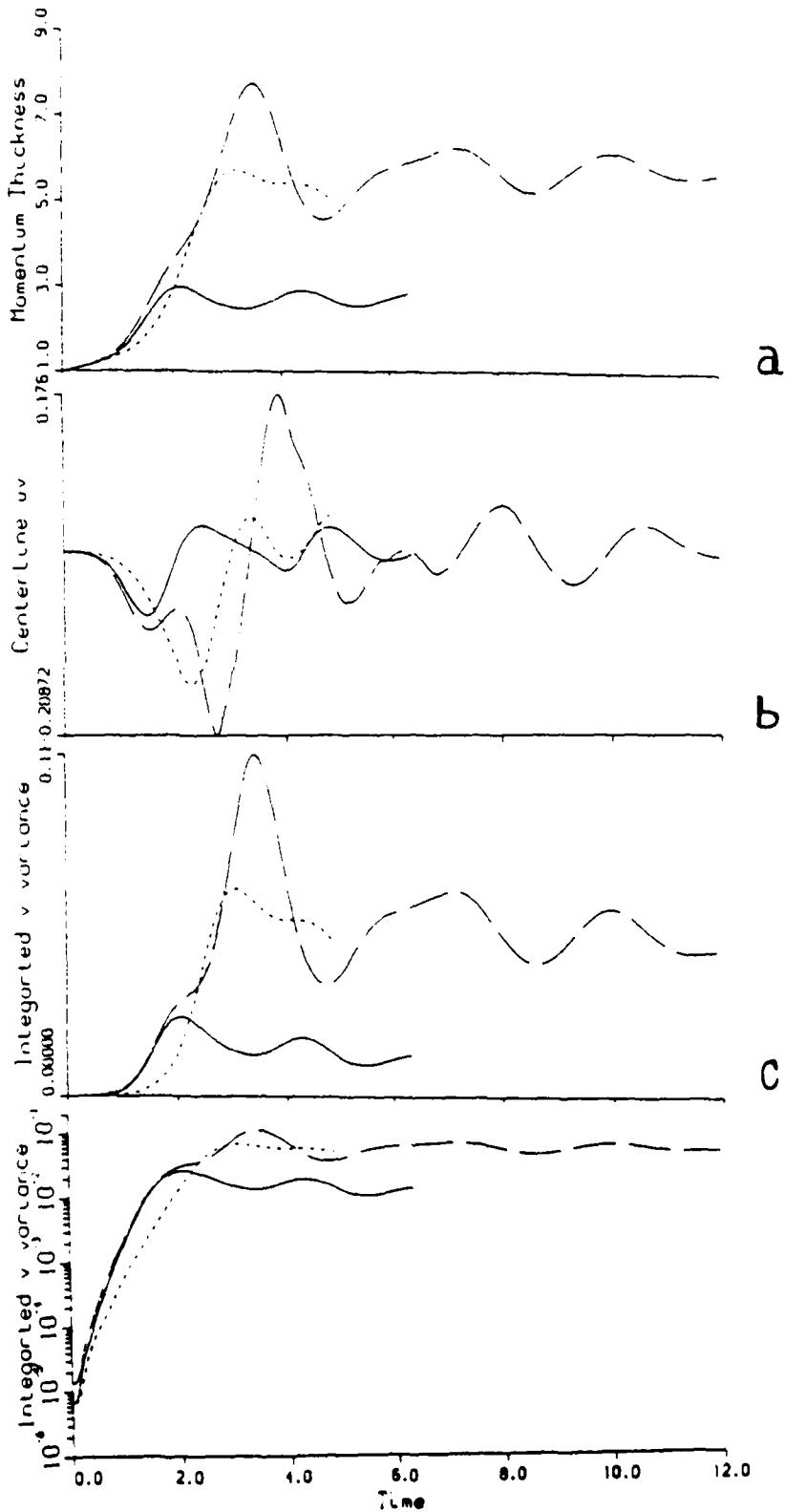
Figure 9 Time history of acoustic variables for vortex roll up; a) Scaled pressure, b) Scaled v ve
c) Reynolds stress work, d) Scaled acoustic flux Solid line ($M_c = 0.2$), Dashed line
0.38) and chained line ($M_c = 0.6$)

Figure 10 Time history of hydrodynamic variables at $M_c = 0.4$; a) Momentum thickness, b) Centerline Reynolds stress, c) Integrated energy in v on linear and log scale. Solid line (fundamental alone), Dashed line (subharmonic alone) and chained line (fundamental and subharmonic

Figure 11 Time history of acoustic variables at $M_c = 0.4$; a) Scaled pressure, b) Calculated acoustic pressure c) Scaled v velocity, d) Reynolds stress work, e) Scaled acoustic flux Solid line (fundamental alone), Dashed line (subharmonic alone) and chained line (fundamental and subharmonic together)

Figure 12 Acoustic radiation from vortex pairing and nutation at $M_c = 0.6$; Time history of a) normalized pressure, b) normalized v velocity, c) Reynolds stress work and d) normalized acoustic flux are shown. Solid line (fundamental alone), Dashed line (fundamental and subharmonic together).

Figure 13 Peak acoustic flux as a function of Mach number M_c; a) fundamental rollup (circles), b) subharmonic rollup (triangles) c) vortex pairing (pluses) and d) vortex shredding (tearing) (cross).

Figure 14 Normalized peak acoustic flux as a function of Mach number M_c; a) fundamental rollup (circles), b) subharmonic rollup (triangles) c) vortex pairing (pluses) and d) vortex shredding (tearing) (cross).

ONR CONTRACT INFORMATION

Contract Title/Principal Investigator: Direct Numerical Simulation/Moin

Contract Number: N00014-88-K-0592

Work Unit Number: 4325-359

Scientific Officer: Lekoudis

Enclosure (1)

Objectives

Use the direct numerical simulations as a tool to study
the noise generation processes directly.

The simulations are used to address the following questions.

- Can one relate particular flow regions and events to the far-field noise ?

- What regions are the dominant contributers to the far-field noise ?

- What is role played by the pairing process in noise generation ?

- How important are the small scales to the noise generation ?

- What processes control the far-field directivity pattern ?

Simulations of compressible mixing layers

Direct numerical simulations of temporally evolving mixing layers were conducted.

- Far-field Acoustic radiation is directly measured.

- Far-field noise is also calculated using the aero-acoustic theory but using the 'exact' source field.
  The exact source field is taken to be the source term in the Lighthill equation.
  It is evaluated directly from the simulations, thus providing the appropriate
  compressiblity effects on the flow field.

Results on Acoustic Radiation from Temporal Mixing Layers

- Verification that hydrodynamic evolution approaches the incompressible limit as $M_c \to 0$.
  where M_c is the convective Mach number.

- For low M_c the measured far-field radiation arising from vortex roll up and pairing behaves
  like M_c^6 as expected from aero-acoustic theory .

- Deviations from the incompressible aero-acoustic limit are obtained as a function of M_c.
  At M_c of 0.2 and 0.5 these deviations are 25% and 100%, respectively.
  The deviations are reduced to 1-2% when the 'exact' source field is used from the simulations.

- Peak noise generated by vortex pairing is about 8-9 times the peak noise generated by vortex roll up.

- Acoustic efficiency is quantified by the simulations. It scales with M^3 for low M.
  Even at M of 0.6 less than 2% of the energy extracted from the mean flow is radiated.

- The slower growth of the compressible mixing layer is not due to the increased acoustic radiation.

Simulation of Acoustic Scattering by vortices

- Small amplitude (10^{-5}) plane sound waves are irradiated on a 'inviscid' vortex $Rc = \frac{\Gamma}{\nu} = 10^5$, $\frac{\lambda}{R_v} = 4$, where Γ is the circulation of the vortex, ν is the kinematic viscosity, λ, is the wavelength of the incident sound waves and R_v the radius of the vortex.

- Scattered sound waves are directly measured and analyzed.

Results on Acoustic Scattering

- Intensity and phase of the scattered field and their dependence on vortex Mach number M_v and $\frac{\lambda}{R_v}$ is obta

- At low M_v far-field intensity scales with the intensity of the incident waves (as predicted by aero-acoustic t

- Deviations from the aero-acoustic limit are quantified. At M_v of 0.25 and 0.5 the deviations are 3% and 25

- Scattering arising from the density inhomogeneity in the vortex is an order of magnitude smaller than the overall scattering.

Future Plans

Computations of 3-D spatially-evolving flows, in particular the near field of a circular jet and a mixing layer.

Computation of the far-field noise characteristics of these flows.

Decomposition of the far-field noise in terms of contributions originating from different spatial regions.

Study the dynamics and acoustics of 'simple' vortex flows to develop a better understanding of the complex flows.

d.

ry).

List of Publications/Reports/Presentations

1. **Papers Published in Refereed Journals:**

   None

2. **Technical Reports:**

   In, Center for Turbulence Research, Annual Research Briefs, 1988, pp. 79-88.

3. **Presentations/**

   a. Invited

   In International Workshop on "The physics of compressible turbulent mixing," Princeton, Nov. 1988.

   b. Contributed

   (1) Paper at AIAA Aerospace Sciences Meeting, Reno, 1989.
   (2) Two papers at APS, DFD Annual Meeting, Palo Alto, Nov. 1989.

4. **Books (and sections thereof):**

   None

Enclosure (2)

LIST OF AWARDS

Name of Person Receiving Award	Recipient's Institution	Name of Award	Sponsor of Award

NONE

Enclosure (3)

PUBLICATIONS/PATENTS/PRESENTATIONS/HONORS REPORT
(Number Only)

Papers Submitted to Refereed Journals (and not yet published):   3

Papers Published in Refereed Journals: None

Papers Published in Non-Referred Journals: None

Technical Reports Published: 1

Books (and sections thereof) Submitted for Publication: None

Books (and sections thereof) Published: None

Patents Filed: None

Patents Granted: None

Invited Presentations at Topical or Scientific/Technical Society Conferences: 1

Contributed Presentations at Topical or Scientific/Technical Society Conferences: 3

Honors/Awards/Prizes: None

Number of Graduate Students: 1

Number of Post Docs: None